MOX–Report No. 12/2011

Tectonic evolution at mid-ocean ridges: geodynamics and numerical modeling

Miglio E.; Cuffaro M.

MOX, Dipartimento di Matematica "F. Brioschi"
Politecnico di Milano, Via Bonardi 9 - 20133 Milano (Italy)

mox@mate.polimi.it http://mox.polimi.it

Tectonic evolution at mid-ocean ridges: geodynamics and numerical modeling

Marco Cuffaro[a], Edie Miglio[b,*]

[a] *IGAG-CNR c/o Dipartimento di Scienze della Terra, Sapienza Università di Roma, P.le A. Moro 5, 00185, Roma, Italy*
[b] *Politecnico di Milano, MOX, Dept. of Mathematics, P.zza L. da Vinci 32, 20133, Milano, Italy*

Abstract

Tectonic evolution at rift zones is commonly considered symmetric along mid-ocean ridges, when modeling with relative plate motions and steady-state processes. However, tectonic features are generally asymmetric, as provided by geological a geophysical data. A better way to understand dynamics of the lithosphere at rift zones, and lithosphere/mantle interactions corresponds to absolute plate kinematic analyses, i.e., with respect to the mantle, modeling time-dependent tectonic processes. We performed numerical simulations of plate-driven mantle flow beneath mid-ocean ridges and we considered a time-dipendent flow induced by the motion of overlying rigid plates in an incompressible viscous mantle, using plate velocities obtained in the hotspot reference frame, as boundary conditions. This implies that plates along a ridge, and the ridge itself, move toward the same direction, but with different velocities, relative to the mantle, and the separation between plates triggers mantle upwelling. Numerical solutions for viscosity flow beneath plates that thicken with increasing age are presented. The mantle can be modeled as a viscous fluid, and its dynamics can be described using the Stokes equations and thermal effects, and a finite element approach has been adopted to obtain numerical solutions. Results show an asymmetric thickening of oceanic plates along the ridge, as suggested by the observations, and provide useful relationships between mantle temperature and thickness of the oceanic lithosphere.

Keywords:
Stationary and transient mid-ocean ridge processes, Mathematical modeling, Computational geodynamics, Numerical approximations and analysis

1. Introduction

Oceanic rift processes are basically due to divergent plate tectonics and plate kinematics. Lithospheric plates, moving apart relative to each others, provide the asthenoshperic mantle upwelling and melting beneath mid-ocean ridges (MORs), supplying new material for the generation of the oceanic crust [1, and references therein]. Spreading centers at the side of MORs

*Politecnico di Milano, MOX, Dept. of Mathematics, tel. +390223994600,
Email address: edie.miglio@polimi.it (Edie Miglio)

represent the areas where to find geophysical and geochemical properties to constrain oceanic lithosphere dynamics, and to investigate lithosphere/mantle interactions.

Since the discovery of magnetic anomalies at sea-bottom of the oceanic basins [2, 3], seafloor spreading has been considered globally symmetric, also if some local asymmetries of the distribution of data were straight after noted in the South Atlantic, Australia and Iceland [4, 5, 6].

During the last two decades, the amount of available data has increased, and data have become better, due to the advances in sea floor imaging, and marine magnetic measurements. In addition, because of both the higher quality of data and the improvements in the models, the asymmetric behavior of tectonic features at MORs are still described, such as the differences in spreading, geometry and subsidence between the two sides of a ridge [7, 8, 9, 10]. Moreover, the bathymetry of MORs, observed at a global scale is generally asymmetric [11, 12], and Doglioni et al. [11] demonstrated that the eastern flank of a ridge, in average, is slightly shallower (100-300 m) than the western one. Based on surface wave tomographic models, shear wave velocities in the upper mantle indicate heterogeneities in the asthenosphere [13, 14], and a difference between the western and eastern flanks of an oceanic basin can be also globally observed across the Earth at MORs [15].

The rift zones and plate boundaries are not fixed, but move with respect to the mantle, and, due to the migration of MORs, some geological and geophysical models can conceptually explain the asymmetries observed [11, 12, 16], also including the global asymmetric behavior of the subduction zones, as a functions of their geographic polarity [17, 18]. The collection of geological, geophysical and geochemical properties at MORs, can be used as constraints for lithosphere/mantle interaction modeling, being useful as boundary conditions, when mantle dynamics is investigated with numerical simulations.

Subridge mantle dynamics is generally modeled as a passive process. Passive mantle upwelling beneath mid-ocean ridges is driven by plate kinematics, and the viscous mantle flow rises beneath the fixed ridge axis, turns a corner and moves away from the upwelling area [19, 20, 21, 22, 23, 24, 25]. In addition, mantle melting, or the presence of the heterogeneities in the mantle composition, can produce buoyancy forces and, in this case, mantle upwelling has to be modeled as an active process. Generally, buoyancy forces are neglected when modeling mantle velocity field, because no remarkable evidence of active flows are observed at spreading centers, and therefore passive models are often used [26].

To have a large comprehension of mantle dynamics, migration of the MORs relative to mantle has to be taken into account. This condition provides more realistic predictions of tectonic processes with results that have a global behavior to understand the evolution of the Earth's surface. In many papers, effects of ridge migration on passive mantle flows have been considered, quantifying, with mathematical models, numerical applications and steady-stade processes, the conceptual and geological models previously proposed [27, 28, 29, 30].

In this paper, we present results of 2D numerical simulations for plate tectonics at MORs, by making use of the MOR–migration condition, passive mantle upwelling models and both steady–state and time-dependent processes. Time-dependent processes need to be introduced to concretely evaluate tectonic evolution at MORs, when the MOR–migration condition is used. To obtain more realistic results, thermal effects were added in the description of the mantle dynamics, and a case for the northern Atlantic Ocean, at mid-Atlantic ridge (MAR), in presented for model comparisons.

2. Geodynamic modeling

The oceanic lithosphere is created at MORs, while two plates are moving away from each other on either side of the fixed ridge (Figure 1a). When the plates diverge, the hot rocks of the underlying mantle, i.e., the asthenosphere, flow upward beneath the MOR, and accrete to the base of the spreading plates, becoming part of them, due to cooling effects by conductive heat loss at the surface. As the plates steadily move away to the oceanic ridge, they continue to be affected by thermal cooling, and the lithosphere thickens.

This type of interaction between the lithosphere and the asthenosphere can be modeled, from a geodynamical point of view, assuming an infinitely thin lithosphere/asthenosphere boundary with a perfectly rigid behaviour of the lithosphere above and uniformly ductile asthenosphere below [e.g., 22, 25]. On the contrary, Shen and Forsyth [23] solved passive mantle flow, adopting a more realistic boundary layer across which the mantle becomes more and more viscous as the plate cools and becomes rigid. The base of lithosphere is assumed to be approximated by the depth of the $T_M = 1350$ °C isotherm, corresponding to a viscosity $\eta = 10^{19}$ Pa s.

A basic step in the geodynamic modeling of MOR evolution corresponds to the choice of plate velocities as boundary conditions. Generally, relative plate motions are often used, where plates move with respect to a fixed ridge axis, with a half spreading velocity V_{hsr} (Figure 1a). Relative plate motions can be measured and are derived by the observations at plate boundaries both with geological data [e.g., 31, 32, 33], or geodetic ones [e.g., 34, 35, 36]. When using these model parameters, mantle flow field is expected to rise under the fixed ridge with a symmetric pattern, and also the accretion of the oceanic lithosphere is predicted to be symmetric (Figure 1a).

On the contrary, when MOR migration is taken into account in the geodynamic models, plate motions referred to the mantle have to be introduced. Mantle-reference (or absolute) motions describe how the entire lithosphere moves relative to the mantle, and they represent a more approrpiate framework for comparisons with results of plate dynamic models. There is not a direct way to measure absolute motions, and they need to be indirectly inferred, using results of relative plate kinematic models.

The hotspot framework is a good reference system, where to evaluate absolute plate motions. It is based on the assumption that the hotspots are fixed relative to the deep mantle and to each other [37, 38], and the orientation and the age progressions along their surface traces reflect the motion of the overlying lithospheric plate relative to the hotspots (e.g., the Hawaiian sea-mount track). Under these assumptions, current global scale plate motions can be computed [39, 40], also if other models of absolute plate motions are defined with different constraints, investigating, for instance, the depth of the source of the hotspots [41], or the hotspot fixity [42, 43]. Then, when using these model parameters, plates and the ridge itself move with different velocities, and the correlated passive mantle flow field is expected to rise under the moving ridge with an asymmetric pattern (Figure 1b). In this case, the accretion of the oceanic lithosphere is predicted to be asymmetric (Figure 1b), being one of flanks of the ridge thicker than the other one.

Here, we consider both the models of passive mantle upwelling beneath a MOR, using relative and aboslute plate motions, as boundary conditions, for stationary and transient plate tectonic processes respectively, to investigate evolution of the spreading centers, and lithosphere/mantle interaction in the ocean basins. The variable viscosity condition proposed by Shen and Forsyth [23] is used in these models, and the computations are applied in the Atlantic Ocean, across the Mid-Atlantic ridge (MAR) representing the boundary between the North America and Eurasia plates, at a reference latitude of 43°N (Figure 2), quantifying the conceptual model proposed by

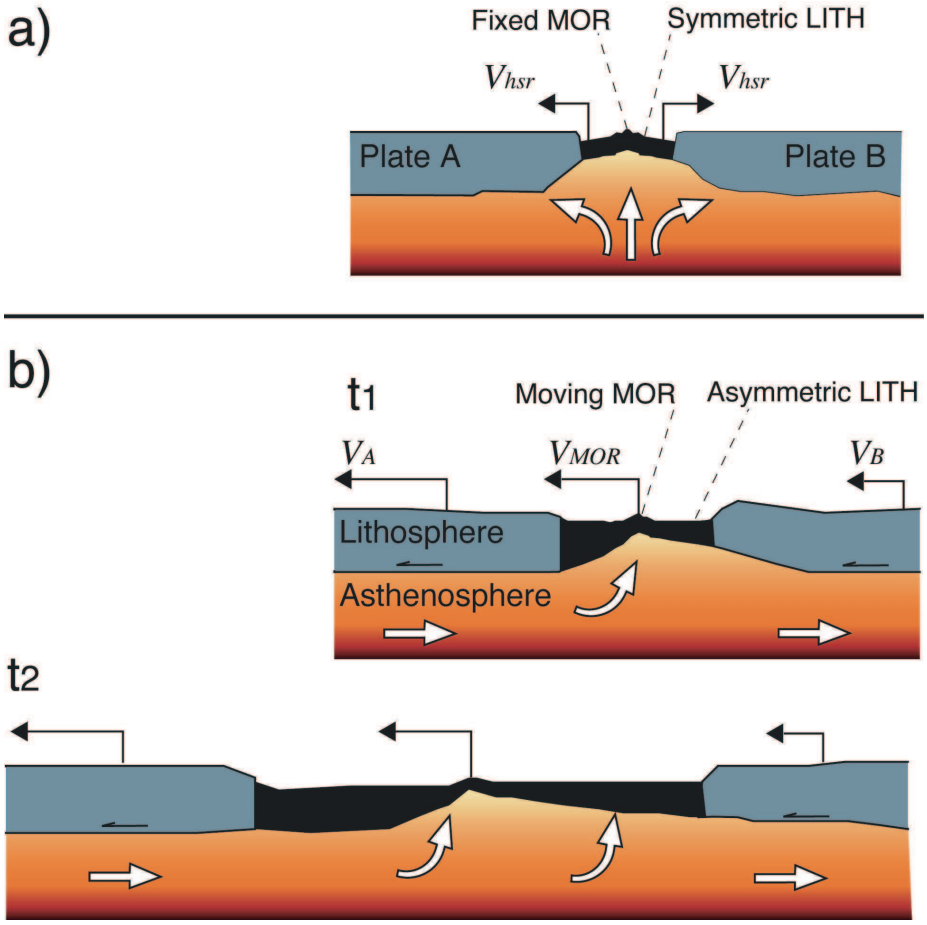

Figure 1: Geodynamic evolution of an oceanic rift at the mid-ocean ridges (MORs). (a) Plates A and B move with respect to the fixed ridge axis of a MOR, with half spreading rate V_{hsr}, providing passive mantle upwelling. The obtained plate-driven mantle flow beneath the MOR is expected to be symmetric, as well as the thickness of the oceanic lithosphere (LITH). (b) Lithospheric plates A and B, and the MOR itself move relative to the asthenoshpere with velocities V_A, V_B, and V_{MOR} respectively, and at different time instants, the separation between plates triggers mantle upwelling, resulting in an asymmetric pattern. In order to make evidence of lithosphere/athenosphere shear, the horizontal components of the velocity field are reported, such that a null horizontal velocity component is obtained on the base of the lithosphere. Thickness of the oceanic lithopshere (LITH) is expected to be asymmetric.

Carminati et al. [16]. In these computations, we use plate-driven mantle upwelling assumptions and thermal effects, not including mantle melting and lateral variations of mantle density, so that we choose to model tectonic evolution at MORs as a passive process.

Physical quantities and parameters adopted in the simulations are reported in Table 1, and we use, at a reference latitude of 43°N, the half spreading rate $V_{hsr} = 10$ mm/a, obtained by

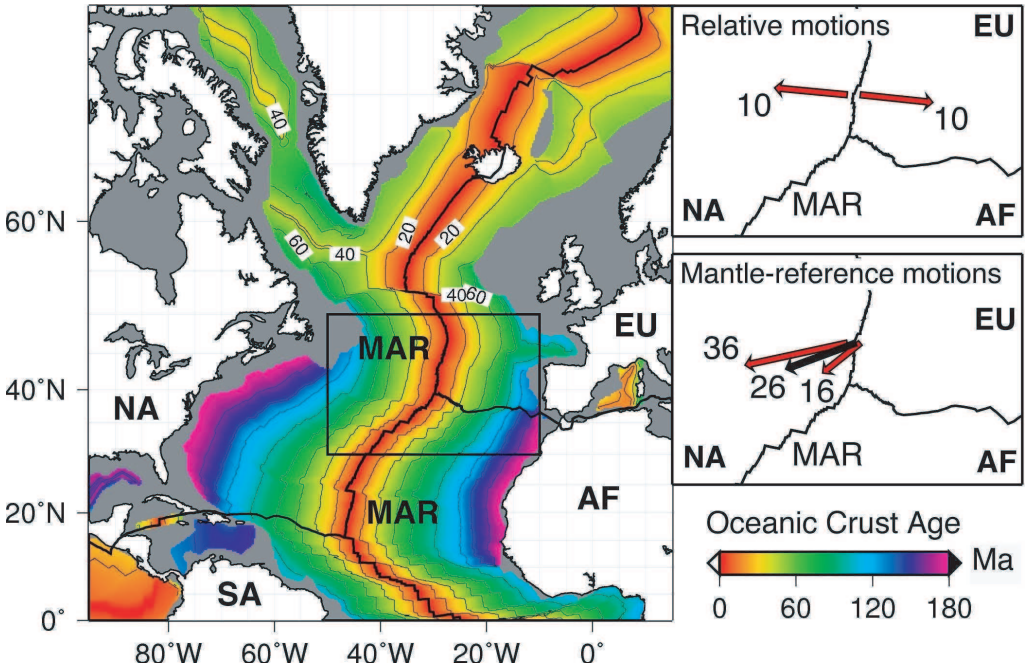

Figure 2: Age of the oceanic crust in the Atlantic Ocean, along the Mid-Atlantic Ridge (MAR). At a reference latitude of 43°N (open box), when considering relative plate motions (upper-right panel) Eurasia (EU) and North America plates (NA), move with respect to the fixed MAR, with half spreading rate V_{hsr} = 10 mm/a (red arrows). On the contrary, at the same latitude, when considering the mantle reference frame, i.e., the hotspots, (lower-right panel) the Eurasia and the North America plates, and the MAR itself move to the west with velocities V_{EU} = 16 mm/a V_{NA} = 36 mm/a (red arrows), and V_{MAR} = 26 mm/a (black arrow) respectively. SA – South Amrerica plate, AF – Africa plate.

DeMets et al. [32] in the ridge axis reference frame, and V_{NA} = 36 mm/a, V_{MAR} = 26 mm/a, and V_{EU} = 16 mm/a for velocities of North America, Mid-Atlantic ridge (MAR), and Eurasia respectively, obtained by Gripp and Gordon [39] in the hotspot framework.

Time-dependent tectonic processes are simulated from 10 Ma up to the Present, during the opening of the Atlantic Ocean, and this condition implies that we investigate the last instants of the evolution of an oceanic rift. This choice is also made because absolute plate motions in the hotspot reference frame obtained by Gripp and Gordon [39] can be considered stable for the last 10 Ma, including error estimates for the hotspots [44]. Moreover, Gordon and Jurdy [45] also used present plate boundary positions and current motions in the hotspot framework to model plate kinematics in the last 10 Ma. In contrast, to go back in the geological past, and to evaluate lithosphere/mantle interactions for different times afterward 10 Ma, reconstruction models for plate tectonics, and appropriate plate kinematic parameters are needed. [e.g., 46].

This temporal condition affects our geodynamic models, such that we first compute the stationary process, and then we use those simulation results as the first step for the transient evolution. Model constraints concerning a time interval Δt = 10 Ma up to Present, and a half spread-

ing rate V_{hsr} = 10 mm/a, correspond to analyze the last term of the Atlantic Ocean opening, in a 200 km wide domain.

3. Mathematical modeling

At first approximation, we can treat the Earth as a fluid, and in particular the lithosphere and the mantle are considered as highly viscous fluids. This amount to use the Navier-Stokes equations to compute the velocity and pressure fields, namely:

$$\rho_M \frac{\partial \mathbf{v}}{\partial t} + \rho_M(\mathbf{v}\cdot\nabla)\mathbf{v} - \rho_M \mathbf{g} = -\nabla p + \nabla\cdot\left[\eta(\nabla\mathbf{v} + \nabla\mathbf{v}^T)\right] \tag{1}$$

$$\nabla\cdot\mathbf{v} = 0, \tag{2}$$

where $\mathbf{v}$ is the velocity, p is the pressure, $\mathbf{g}$ is the gravity acceleration, ρ_M is the mantle density.

Moreover in (1), η is the variable viscosity of the fluid, which is a complex function depending on temperature, pressure, strain, compostion etc.; in [47] the following law has been proposed:

$$\eta = \frac{1}{2A}\left(\frac{\mu}{\tau}\right)^{(n-1)}\left(\frac{h}{b^*}\right)^m \exp\frac{E^* + PV^*}{RT}, \tag{3}$$

where A is a constant, μ is the shear modulus, b^* is the Burgers vector, T is the temperature, τ is the second invariant of the deviatoric stress tensor, E^* is the activation energy, V^* is the activation volume, R is the gas constant, h is the grain size, n is a stress exponent, and m a grain-size exponent. This relation is quite difficult, but the most important effect on the viscosity, on the space and time scales considered, is the temperature effect. Hence, using the the Frank-Kamenetskii approximation, following McKenzie [48] and Solomatov [49], we can simplify (3) as follow:

$$\eta = A' \exp\left(-C\frac{T}{T_M}\right), \tag{4}$$

where T_M is a reference temperature, i.e., the mantle temperature; in the numerical simulations we will use the following law [50]:

$$\eta = 10^{24}\exp\left(-11.5129\frac{T}{T_M}\right). \tag{5}$$

The temperature field T is diffused and advected by the transport field $\mathbf{v}$:

$$\rho_M c_p\left(\frac{\partial T}{\partial t} + (\mathbf{v}\cdot\nabla)T\right) = \nabla\cdot(k\nabla T), \tag{6}$$

where c_p is the specific heat capacity and k is the thermal conductivity; the ratio

$$\kappa = \frac{k}{\rho_M c_p} \tag{7}$$

is the so called thermal diffusivity.

Actually, we are in a situation in which the Prandtl number:

$$Pr = \frac{\eta}{\kappa} \tag{8}$$

is very high (10^{26}, see Table 1), and hence the inertial terms in (1) can be neglected, so that a generalized Stokes problem is usually adopted:

$$-\nabla p + \nabla \cdot \left[\eta(\nabla \mathbf{v} + \nabla \mathbf{v}^T)\right] = -\rho_M \mathbf{g}, \tag{9}$$

$$\nabla \cdot \mathbf{v} = 0. \tag{10}$$

In practice, from the fluid dynamics point of view, we have a sequence of steady states, and the temporal evolution is only due to the temporal variation of the temperature field.

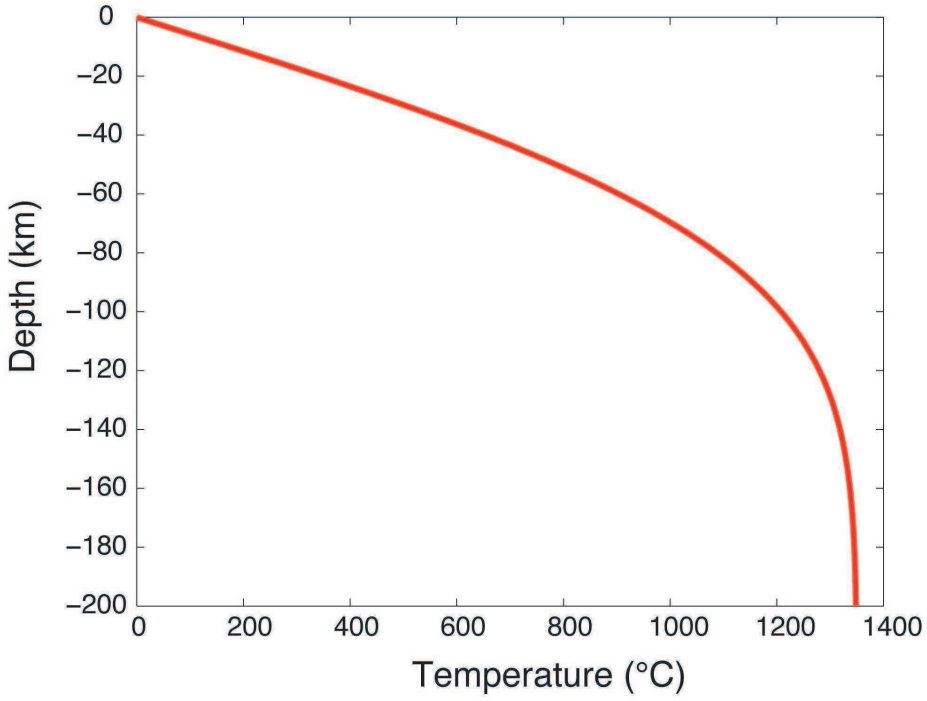

Figure 3: The mean oceanic geotherm, computed with the equation (11), is used as the initial state for mantle temperature T, to obtained numerical solutions.

The system (9)-(10)-(6) has to be supplied by suitable boundary conditions, and by an initial condition for the temperature field. Figure 3 shows the thermal profile, i.e., the mean oceanic geotherm, used as initial condition for the temperature; the analytic expression of this profile is given in Schubert et al. [51] and reads as follows:

$$\frac{T(z) - T_M}{T_M - T_0} = \operatorname{erf}\left(\frac{z}{2\sqrt{\kappa \mathcal{T}}}\right), \tag{11}$$

where z is the depth variable and $\mathcal{T}$ is the sea floor mean age [52].

The particular choice of initial and boundary conditions used in the simulation are described in Figure 4. In particular, on the bottom of the cartesian domain, the velocity and the stress are assumed to be normal to the boundary. On the lateral boundaries, a velocity profile normal to the

boundary is imposed, depending on the choice of the plate kinematic framework. On the top, the tangential component of the velocity is assigned and the normal component is zero. As for the temperature, on the lateral boundaries a zero thermal flux is imposed, whereas the temperature is assigned on the top and on the bottom of the domain. In the next sections the following notation will be used:

- Dirichlet boundary for Stokes Γ_{DS} = top and lateral;
- Neumann boundary for Stokes Γ_{NS} = bottom;
- Dirichlet for the temperature Γ_{DT} = top and bottom;
- Neumann for the temperature Γ_{NT} = lateral.

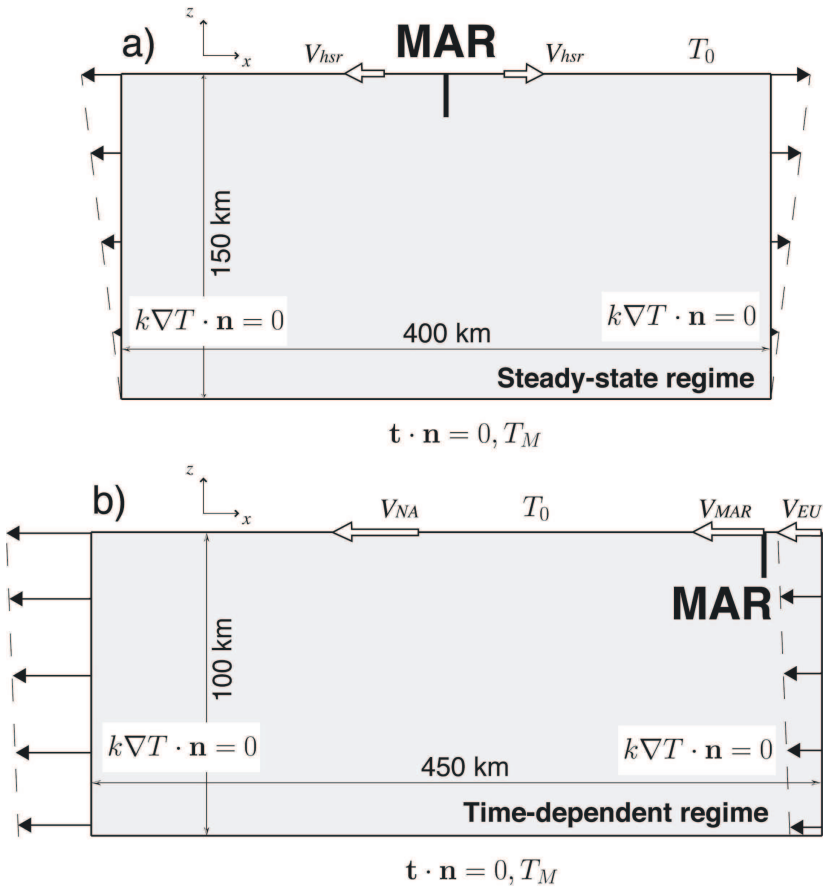

Figure 4: Model setup and boundary conditions for numerical simulations for (a) steady-state regime and (b) time-dependent regime. Physical quantities are reported in Table 1. On the lateral boundaries, and on the lower boundary a convective heat flux, and a normal velocity flow are imposed, respectively.

Table 1: Physical quantities and parameters used for model computations.

Parameter	Description	Value	Units
V_{hsr}	Half spreading rate	10	$\mathrm{mm\,a^{-1}}$
V_{NA}	North America hotspot velocity	36	$\mathrm{mm\,a^{-1}}$
V_{EU}	Eurasia hotspot velocity	26	$\mathrm{mm\,a^{-1}}$
V_{MAR}	Mid-Atlantic ridge migration rate	16	$\mathrm{mm\,a^{-1}}$
ρ_M	Mantle density	3300	$\mathrm{kg\,m^{-3}}$
η	Variable mantle viscosity	$10^{19} - 10^{24}$	Pa s
g	Gravity accelaration	9.81	$\mathrm{m\,s^{-2}}$
c_p	Mantle heat capacity	1350	$\mathrm{J\,kg^{-1}\,K^{-1}}$
k	Mantle thermal conductivity	3.3	$\mathrm{W\,m^{-1}\,K^{-1}}$
κ	Mantle thermal diffusivity	7.4×10^{-7}	$\mathrm{m^2\,s^{-1}}$
T_0	Surface temperature	0	°C
T_M	Mantle temperature	1350	°C
$\mathcal{T}$	Sea floor mean age	60	Ma

4. Time advancing scheme

The evolution in time is only due to the time derivative in the advection-diffusion equation for the temperature; as for the Stokes equations, a steady problem has to be solved at each time step, using a viscosity field depending on the computed temperature.

From the numerical point of view, the solution of the coupled Stokes - temperature system, namely equations (9)-(10) and (6), amounts to adopt the following iterative procedure:

1. given the initial state T^0 for the temperature, compute the viscosity field η^0;
2. new time step $t^{n+1} = t^n + \Delta t$;
3. solve the Stokes problem in the unknowns $(\mathbf{v}^{n+1}, p^{n+1})$, namely

$$-\nabla p^{n+1} + \nabla \cdot \left[\eta^n (\nabla \mathbf{v}^{n+1} + (\nabla \mathbf{v}^{n+1})^T)\right] = -\rho_M \mathbf{g}, \tag{12}$$

$$\nabla \cdot \mathbf{v}^{n+1} = 0. \tag{13}$$

4. solve for the temperature T^{n+1}, using the velocity field $\mathbf{v}^{n+1}$, i.e.

$$\rho_M c_p \left(\frac{T^{n+1} - T^n}{\Delta t} + (\mathbf{v}^{n+1} \cdot \nabla) T^{n+1} \right) = \nabla \cdot (k \nabla T^{n+1}), \tag{14}$$

   where the implicit Euler scheme is adopted for the time advancing.
5. compute the new viscosity field η^{n+1} at time t^{n+1}, and go to step 2.

5. Space discretization

Let Ω be the 2D domain of interest, and $L^2(\Omega)$ the Lebesgue space; we will also use the following notation:

$$H^1(\Omega) = \left\{ v \in L^2(\Omega),\ \frac{\partial v}{\partial x_i} \in L^2(\Omega) \text{ for } i = 1, 2 \right\}; \tag{15}$$

$$H^1_{0,\Gamma_{DS}}(\Omega) = \left\{ v \in H^1(\Omega),\ v|_{\Gamma_{DS}} = 0 \right\}; \tag{16}$$

$$H^1_{0,\Gamma_{DT}}(\Omega) = \left\{ v \in H^1(\Omega),\ v|_{\Gamma_{DT}} = 0 \right\}; \tag{17}$$

$$H^{1/2}(\Gamma_{DS}) = \left\{ \xi \in L^2(\Gamma_{DS}),\ \exists v \in H^1(\Omega),\ v|_{\Gamma_{DS}} = \xi \right\}; \tag{18}$$

$$H^{1/2}(\Gamma_{DT}) = \left\{ \xi \in L^2(\Gamma_{DT}),\ \exists v \in H^1(\Omega),\ v|_{\Gamma_{DT}} = \xi \right\}. \tag{19}$$

The following vector space will be used as well

$$\mathbf{H}^1_{0,\Gamma_{DS}} = H^1_{0,\Gamma_{DS}} \times H^1_{0,\Gamma_{DS}} \tag{20}$$

Let us define the following bilinear forms

$$\mathbf{a}(\mathbf{v}, \mathbf{u}; \eta) = \int_\Omega \eta(\nabla \mathbf{v} + \nabla \mathbf{v}^T) : (\nabla \mathbf{u} + \nabla \mathbf{u}^T), \tag{21}$$

$$a(T, \varphi) = \int_\Omega k \nabla T \cdot \nabla \varphi, \tag{22}$$

$$b(T, \varphi; \mathbf{v}) = \int_\Omega (\mathbf{u} \cdot \nabla) T \varphi. \tag{23}$$

Then, at each time step, we have the following weak problem:

given $\mathbf{v}_D \in \mathbf{H}^{1/2}(\Gamma_{DS})$, and $T_D \in H^{1/2}(\Gamma_{DT})$, find $(\mathbf{v}^{n+1}, p^{n+1}, T^{n+1}) \in \mathbf{H}^1(\Omega) \times L^2(\Omega) \times H^1(\Omega)$ such that $\mathbf{v}|_{\Gamma_{DS}} = \mathbf{v}_D$, and $T|_{\Gamma_{DT}} = T_D$ solution of

$$\mathbf{a}(\mathbf{v}^{n+1}, \mathbf{u}, \eta^n) + (\nabla \cdot \mathbf{u}, p^{n+1})_{0,\Omega} = (-\rho_M \mathbf{g}, \mathbf{u})_{0,\Omega}, \qquad \forall \mathbf{u} \in \mathbf{H}^1_{0,\Gamma_{DS}} \tag{24}$$

$$(\nabla \cdot \mathbf{v}^{n+1}, q)_{0,\Omega} = 0, \qquad \forall q \in L^2(\Omega) \tag{25}$$

$$\frac{\rho_M c_P}{\Delta t}(T^{n+1}, \varphi)_{0,\Omega} + a(T, \varphi) + \rho_M c_p b(T, \varphi, \mathbf{v}^{n+1}) = \frac{\rho_M c_P}{\Delta t}(T^n, \varphi)_{0,\Omega}, \qquad \forall \varphi \in H^1_{0,\Gamma_{DT}} \tag{26}$$

6. Numerical approximation

The domain of interest has been discretized using a non-uniform triangular mesh, and for the solution of the Stokes equations, standard Lagrange $\mathbb{P}_2$ finite elements for the velocity and $\mathbb{P}_1$ for the pressure have been employed respectively.

The algebraic system deriving from this discretization can be formally written as:

$$\underbrace{\begin{bmatrix} K & D \\ D^T & 0 \end{bmatrix}}_{\mathcal{M}} \begin{bmatrix} \mathbf{u}_h \\ \mathbf{p}_h \end{bmatrix} = \begin{bmatrix} \mathbf{f} \\ \mathbf{g} \end{bmatrix} \tag{27}$$

where K and D are the algebraic counterpart of the Laplace and gradient operators; $\mathbf{u}_h$ and $\mathbf{p}_h$ are the vectors containing the nodal values for the velocities and for the pressure; $\mathbf{f}$ and $\mathbf{g}$ are the right-had-side vectors depending on the boundary conditions. The algebraic problem has been

solved usign a preconditioned Krylov method. The preconditioner has been chosen according to [53] i.e.

$$\hat{\mathcal{M}} = \begin{bmatrix} \hat{K} & 0 \\ 0 & -\hat{S} \end{bmatrix} \tag{28}$$

where $S = D^T K^{-1} D$ is the Schur complement and $\hat{S}$ is a preconditioner for the Schur complement. In practice we took

$$\hat{K} = \begin{bmatrix} K_{11} & 0 \\ 0 & K_{22} \end{bmatrix} \tag{29}$$

where K_{ii}, $i = 1, 2$ are the diagonal blocks of the stiffness matrix K; matrix $\hat{K}$ corresponds the following bilinear form

$$\hat{\mathbf{a}}(\mathbf{v}, \mathbf{u}; \eta) = \int_\Omega \eta \nabla \mathbf{v} : \nabla \mathbf{u}, \tag{30}$$

which is spectrally equivalent to $\mathbf{a}(\mathbf{v}, \mathbf{u}; \eta)$.

Moreover $\hat{S} = M_\eta$ is a scaled pressure matrix i.e. $(M_\eta)_{i,j} = (\eta^{-1} p_j, q_i)_{0,\Omega}$.

As for the transport diffusion equation for the temperature, $\mathbb{P}_2$ finite elements have been used along with SUPG stabilization.

7. Results and discussion

Results of 2D numerical simulations show substantial differences when modeling with a steady–state approach or a time–dependent one. Moreover these differences are also linked to the choice of the kinematic framework, i.e., relative versus mantle–reference plate motions.

Figure 5 refers to the numerical simulations in the Atlantic Ocean, by making use of a steady-state regime for viscosity flow beneath plates that thicken with increasing age. The MAR is assumed to be fixed, and passive mantle velocity field results in a symmetric pattern; as for the temperature a similar symmetric behaviour is obtained. The base of the lithosphere, corresponding to the depth of the line 19.1 of the $\log_{10}(\eta)$, is symmetric as well, with a minimum depth of -92 km on lateral boundaries, and a maximum one of -10 km beneath the ridge axis, in the whole domain of the simulation (400 km). Considering the opening of the Atlantic Ocean at the reference latitiude of investigations (i.e., 43°N), which amounts to take into account a domain of 200 km in a time interval of 10 Ma, the minimum depth of the base of the lithosphere is -48 km. At that depth below the ridge axis, the vertical component of the mantle upwelling ($V \approx 12$ mm/a) is higher than the half spreading rate V_{hsr} due to the fact that the flow field is close to the narrowing region, where the lithosphere thickens, as also noted by Shen and Forsyth [23]. The thickening of high viscosity layer at the surface forces mantle flow field to be faster to supply material that moves horizontally away from the spreading ridge axis [23].

Significant different results are obtained when computing evolution of MORs using a time-dependent approach, and mantle-reference velocities as boundary conditions. Starting from the solution computed using the steady-state approach, the evolution during the last 10 Ma is simulated, and an asymmetric thickening of the lithosphere is observed (see Figure 6). In this second case, the MAR migrates relative to the mantle during the opening of tha Atlantic Ocean, and plates move with different velocities. These conditions trigger mantle upwelling beneath the MAR, and the obtained mantle flow field is asymmetric (Figure 6).

In order to emphasize the shear between the lithosphere and the astenosphere, the horizontal components of the velocity field have been recalculated such that a null horizontal velocity

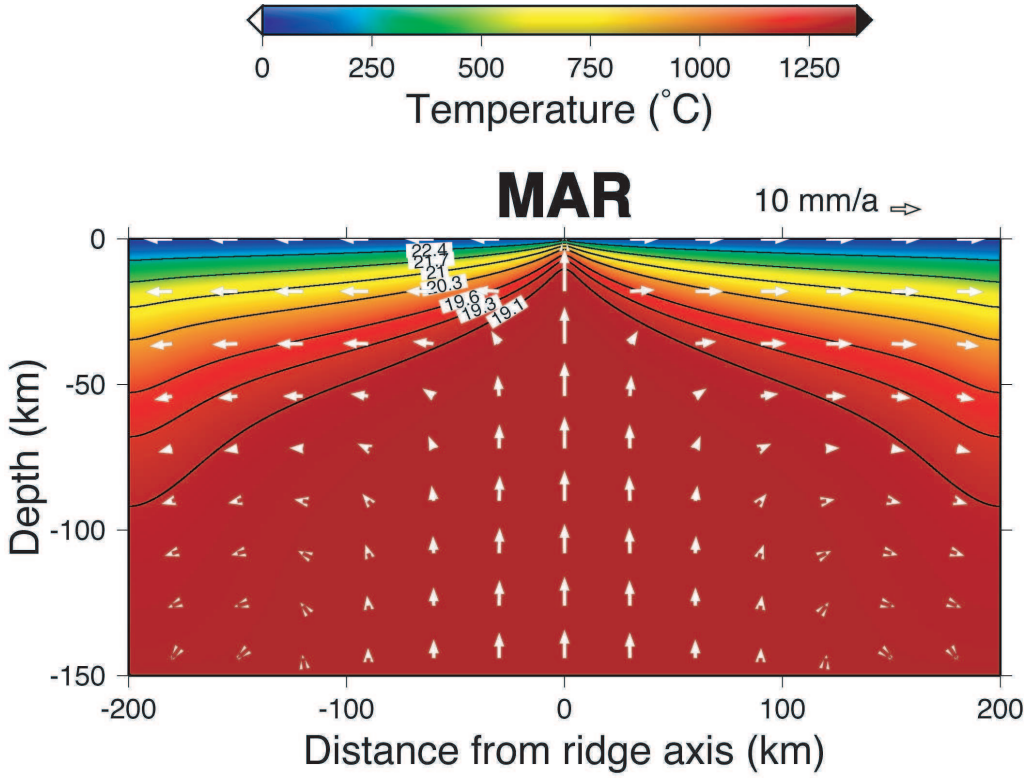

Figure 5: Results of numerical simulations in a steady-state regime for viscosity flow beneath plates that thicken with increasing age. The Mid-Atlantic ridge (MAR) is fixed and passive mantle velocity field (white arrows) is symmetric. Colors are related to the distribution of the temperature. Contour lines represent the Log of the temperature dependent viscosity. The transition between the lithosphere and asthenosphere is assumed to correspond in our calculations to the depth of the line 19.1, that results in a symmetric shape.

component is obtained on the base of the lithosphere, i.e., the line 19.1 of the $\log_{10}(\eta)$. This configuration shows that the North-America and Eurasia plates, and the MAR itself, are moving toward the west, whereas the mantle relatively flows toward the east. During the evolution of the last 10 Ma for the Atlantic Ocean, the mantle flow rises upward beneath the migrating spreading center, contributing to an asymmetric accretion of the lithosphere. This asymmetric shape is a direct consequence of the asymmetric pattern of the temperature field. Considering as above the 200 km domain, at the final stage (the Present), the base of the lithosphere reaches two different depths: approximately -57 km on the western flank (North America) and -44 km on the eastern one (Eurasia), providing a different thickness of the lithosphere at the two sides of the ridge.

The vertical component of the mantle upwelling at the depth of -48 km below the ridge axis at 8 Ma is equal to approximately 11 mm/a (Figure 6). Although this value is similar to the stationary case, it continues to be higher compared with the half spreading rate. This effect can be explained observing that the geometry of the oceanic plates is still narrow in the region of

spreading center after 2 Ma of evolution. As the simulation progresses, the narrowing of this region is less evident, and at the final step (the Present), the base of the lithosphere beneath the MAR is 31 km deep, and this value shows a higher thickness than the stationary case; at this final stage the vertical component recorded at -48 km depth is 5 mm/a (Figure 6).

With the purpose to quantitatively evaluate the whole simulations, a comparison on the shape of the lithosphere-asthenosphere transition obtained in the two models (i.e. steady-state versus transient) is reported in Figure 7. Linear least-square Łfit of the curve flanks at the base of the lithosphere were performed in the 200 km domain for the Present. Considering the steady-stae case, a symmetric shape is obtained with a slope of 0.37, whereas, in the time dependent simulation, an asymmetric result is computed, showing a slope of 0.25 for the western flank (North America) and 0.12 for the eastern one (Eurasia).

The asymmetric thickness of the lithosphere resulting from the time-dependent simulation is in good agreement with the geological data, based on surface wave tomography models, globally observed at MORs [15]. Moreover, shear wave velocities in the upper mantle also suggest that, beneath the MAR, an high value of the thickness of the lithosphere is observed [54, 15]. Our transient simulations for the Present show that the thickness of the lithosphere beneath the MAR is higher than the one obtained in the stationary case (31 km versus 10 km); this higher value seems to be in agreement with the available data, even if it is quite different from the one expected using a steady-state approach. Moreover, additional geophysical data, obtained by models of global lithospheric thickness computations [e.g., 55, 56], seems to confirm a depth of -20 or -30 km for the lithosphere/athenosphere transition beneath the MAR. In addition, Grad et al. [57] reported a Moho depth of 10 km at the latitude of our investigation, and this could suggest a higher depth for the base of the lithosphere.

We expect that the inclusion in the model of lateral density variations and melting processes, which have not been considered in this study, could modify the thickness of the lithosphere beneath the MAR, providing an higher value for the depth of the lithosphere/asthenosphere transition, and a useful relationship between mantle temperature and thickness of the oceanic lithosphere.

8. Concluding remarks

We have performed 2D numerical simulations for temperature–dependent mantle viscosity flow field beneath lithospheric plates that thicken with age, evaluating tectonic evolution at mid-ocean ridges (MORs), useful to investigate the geometry of mantle upwelling and lithospheric thickness.

Results show a significant difference when modeling with relative or absolute plate motions as boundary conditions, using stationary or transient processes respectively. The use of steady-state regime results in a symmetric mantle flow, temperature distribution, and thickness of the lithosphere, whereas, for the time-dependent case, an asymmetric flow pattern, temperature field, and plate thickness are obtained. When two plates and the MOR itself move in the same directionwith respect to the hotspot reference frame, i.e, toward the west in our model, the lithosphere on the western flank of the ridge is thicker than the eastern one.

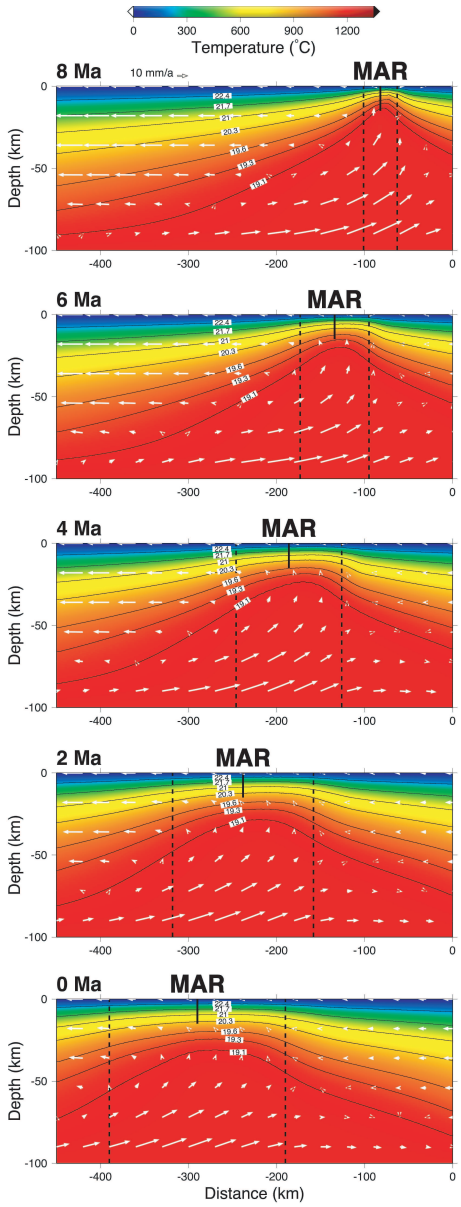

Figure 6: Results of numerical simulations in a time-dependent regime for viscosity flow beneath plates that thicken with increasing age, in a time interval from 10 Ma up to the Present. The initial state at 10 Ma corresponds to the stationary results of the figure 5. Colors are related to the distribution of the temperature, and contour lines represent the Log of the temperature dependent viscosity. The transition between the lithosphere and asthenosphere is assumed to correspond to the depth of the 19.1, that results in an asymmetric shape, during the opening of the atlantic ocean (dashed lines). The Mid-Atlantic ridge (MAR) is moving toward the west, and passive mantle velocity field scaled on the contour line 19.1 (white arrows) is asymmetric.

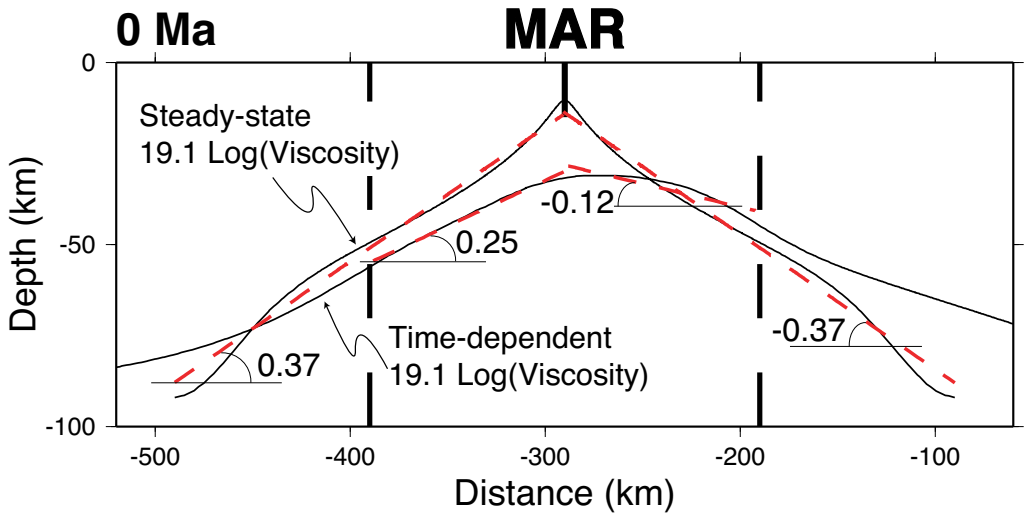

Figure 7: Comparison of the shape of the transition between the lithosphere and asthenosphere, corresponding to depth of the contour line 19.1 ($\log_{10}(\eta)$), for steady-state and time-dependent regime in the last 10 Ma, respectively. Linear least-square Łfit of the curve flanks at the base of the lithosphere (line 19.1) shows a symmetric result in the steady-state regime with a slope of 0.37, whereas shows an asymmetric result for the time-dependent regime (0.25 versus 0.12).

Because of the more appropriate use of absolute plate motions to understand plate tectonic dynamics, and lithosphere/mantle interactions, the transient processes and absolute motions as boundary conditions represent a better choice to investigate the evolution of the Earth's surface. Under these assumpions, the results obtained seems to be in agreement with the observations at rift zones, such as the topography differences [11, 12], or the lithospheric thickness asymmetries [15], and support some global models for plate tectonics and plate kinematics, i.e., the westward drift of the lithosphere [58, 59, 60, 41, 18].

Moreover, it is useful to emphasize the shear between the lithosphere an the asthenosphere, considering mantle upwelling referred to the base of the lithosphere. The upward flow field reported in Figure 6 shows an asymmetric vertical distribution of velocities at MAR, mainly oriented toward the plate standing on the eastern side of the ridge, i.e., the Eurasia. This could suggest a correlation between the mantle processes at rift zones and the uplift and crustal deformations occurring on the eastern plate, as shown for the Eurasia plate by Nielsen et al. [61] and Carminati et al. [16].

The addition of further constraints in the models, such as the spherical geometry, the density variations as a function of temperature and composition, and mantle melting processes, could emphasize the asymmetries observed in this paper, and could support to explain, with more realistic details, tectonic evolution at MORs. The introduction of temperature-dependent density and the physics of mantle melting implies to consider a buoyant flow, and to model mantle upwelling as an active process. Flow patterns strongly affect mantle thermal structure and melt production beneath a spreading centre, and the combination of passive and active mantle dynamics could contribute to the knowledge of the relationships among mantle thermal pattern, melt production, geochemistry of erupted lavas, and thickeness of the lithosphere at rift zones.

Acknowledgments

We extend many thanks for suggestions and stimulating discussions to Marco Ligi, Eugenio Carminati, Luca Formaggia, and Carlo Doglioni. Many of the figures were made with the Generic Mapping Tools of Wessel and Smith [62].

References

[1] Cann JR, Elderfield H, Laughton AS. Mid-ocean ridges, dynamics of processes associated with the creation of new oceanic crust. Cambridge University Press; 1999.
[2] Vine FJ, Matthews DH. Magnetic anomalies over oceanic ridges. Nature 1963;199:947–9.
[3] Vine FJ. Spreading of the ocean floor: new evidence. Science 1966;154:1405–15.
[4] Dickson GL, Pitman WC, Heirtzler JR. Magnetic anomalies in the South Atlantic and ocean floor spreading. J Geophys Res 1968;73:2087–100.
[5] Weissel JK, Hayes DE. Asymmetric spreading south of Australia. Nature 1971;231:518–22.
[6] Johnson GL, Southall JR, Young PW, Vogt PR. Origin and structure of the Iceland Plateau and Kolbeinsey ridge. J Geophys Res 1972;77:5688–96.
[7] Morgan JP, Smith WHE. Flattening of the sea-floor depth-age curve as a response to asthenospheric flow. Nature 1992;359:524–7.
[8] Cande SC, Kent DV. Revised calibration of the geomagnetic time scale for the Late Cretaceous and Cenozoic. J Geophys Res 1995;100:6093–5.
[9] Bonatti E, Ligi M, Brunelli D, Cipriani A, Fabretti P, Ferrante V, et al. Mantle thermal pulses below the mid-atlantic ridge and temporal variations in the formation of oceanic lithosphere. Nature 2003;423:499–505.
[10] Müller RD, Sdrolias M, Gaina C, Roest WR. Age, spreading rates and spreading asymmetry of the worlds ocean crust. Geochem Geophys Geosyst 2008;9. doi:10.1029/2007GC001743.
[11] Doglioni C, Carminati E, Bonatti E. Rift asymmetry and continental uplift. Tectonics 2003;22. doi:10.1029/2002TC001459.
[12] Carbotte SM, Small C, Donnelly K. The influence of ridge migration on the magmatic segmentation of mid–ocean ridges. Nature 2004;429:743–6.
[13] Zhang YS, Tanimoto T. High-resolution global upper mantle structure and plate tectonics. J Geophys Res 1993;98:9793–823.
[14] Calcagno P, Cazenave A. Subsidence of the seafloor in the Atlantic and Pacific oceans; regional and large-scale variations. Earth Planet Sci Lett 1994;126:473–92.
[15] Panza G, Doglioni C, Levshin A. Asymmetric ocean basins. Geology 2010;38:59–62.
[16] Carminati E, Cuffaro M, Doglioni C. Cenozoic uplift of Europe. Tectonics 2009;28. doi:10.1029/2009TC00247.
[17] Doglioni C, Carminati E, Cuffaro M. Simple kinematics of subduction zones. Int Geol Rev 2006;48:479–93.
[18] Doglioni C, Carminati E, Cuffaro M, Scrocca D. Subduction kinematics and dynamic constraints. Earth Sci Rev 2007;83:125–75.
[19] McKenzie D. Speculations on the consequences and causes of plate motion. Geophys J R Astron Soc 1969;18:1–32.
[20] Reid I, Jackson HR. Oceanic spreading rate and crustal thickness. Mar Geophys Res 1981;5:165–72.
[21] Morgan JP, Forsyth DW. Three–dimensional flow and temperature perturbations due to a transform offset: effects on oceanic crustal and upper mantle structure. J Geophys Res 1988;93:2955–66.
[22] Blackman DK, Forsyth DW. The effects of plate thickening on three-dimensional, passive flow of the mantle beneath mid-ocean ridges. In: Morgan JP, Blackman DK, Sinton JK, editors. Mantle Flow and Melt Generation at Mid-Ocean Ridges; vol. 71. AGU Geophysical Monograph; 1992, p. 311–26.
[23] Shen Y, Forsyth DW. The effects of temperature and pressure dependent viscosity on three–dimensional passive flow of the mantle beneath a ridge–transform system. J Geophys Res 1992;97:19717–28.
[24] Behn MD, Boettcher MS, Hirth G. Thermal structure of oceanic transform faults. Geology 2007;35:307–10.
[25] Ligi M, Cuffaro M, Chierici F, Calafato A. Three–dimensional passive mantle flow beneath midocean ridges: an analytical approach. Geophys J Int 2008;175:783–805.
[26] Spiegelman M, Reynolds JR. Combined dynamic and geochemical evidence for convergent melt flow beneath the east pacific rise. Nature 1999;402:282–5.
[27] Stein S, Melosh HJ, Minster JB. Ridge migration and asymmetric sea–floor spreading. Earth Planet Sci Lett 1977;36:51–62.
[28] Davis EE, Karsten JL. On the cause of the asymmetric distribution of seamounts about the juan de fuca ridge–ridge–crest migration over a heterogeneous asthenosphere. Earth Planet Sci Lett 1986;79:385–96.

[29] Katz RF, Spiegelman M, Carbotte SM. Ridge migration, asthenospheric flow and the origin of magmatic segmentation in the global mid–ocean ridge system. Geophys Res Lett 2004;31. doi:10.1029/2004GL020388.
[30] Weatherley SM, Katz RF. Plate–driven mantle dynamics and global patterns of mid–ocean ridge bathymetry. Geochem Geophys Geosyst 2010;11. doi:10.1029/2010GC003192.
[31] Minster JB, Jordan TH. Present-day plate motions. J Geophys Res 1978;83:5331–54.
[32] DeMets C, Gordon RG, Argus DF, Stein S. Effect of recent revisions to the geomagnetic reversal time scale on estimates of current plate motions. Geophys Res Lett 1994;21:2121–94.
[33] DeMets C, Gordon RG, Argus DF. Geologically current plate motions. Geophys J Int 2010;181:1–80.
[34] Gordon RG, Stein S. Global tectonics and space geodesy. Science 1992;256:333–42.
[35] Argus DF, Heflin MB. Pate motion and crustal deformation estimated with geodetic data from Global Positionig System. Geophys Res Lett 1995;22:1973–6.
[36] Altamimi Z, Collilieux X, Legrand J, Garayt B, Boucher C. ITRF2005: A new release of the International Terrestrial Reference Frame based on time series of station positions and Earth Orientation Parameters. J Geophys Res 2007;112. doi:10.1029/2007JB004949.
[37] Morgan WJ. Convection plumes in the lower mantle. Nature 1971;230:42–3.
[38] Wilson JT. Mantle plumes and plate motions. Tectonophysics 1973;19:149–64.
[39] Gripp AE, Gordon RG. Young tracks of hotspots and current plate velocities. Geophys J Int 2002;150:321–64.
[40] Cuffaro M, Jurdy DM. Microplate motions in the hotspot reference frame. Terra Nova 2006;18:276–81.
[41] Cuffaro M, Doglioni C. Global kinematics in deep versus shallow hotspot reference frames. In: Foulger GR, Jurdy DM, editors. The Origins of Melting Anomalies: Plumes, Plates, and Planetary Processes; vol. 430. Geol. Soc. Am. Sp. Paper; 2007, p. 359–74.
[42] Torsvik TH, der Voo RV, Redeld TF. Relative hotspot motions versus true polar wander. Earth Planet Sci Lett 2002;202:185–200.
[43] ONeill C, Müller D, Steinberger B. On the uncertainties in hot spot reconstructions and the significance of moving hot spot reference frames. Geochem Geophys Geosyst 2005;6. doi:10.1029/2004GC000784.
[44] Jurdy DM. Reference frames for plate tectonics and uncertainties. Tectonophysics 1990;182:373–82.
[45] Gordon RG, Jurdy DM. Cenozoic global plate motions. J Geophys Res 1986;91:12384–406.
[46] Torsvik T, Müller RD, der Voo RV, Steinberger B, Gaina C. Global plate motion frames: Toward a unified model. Rev Geophys 2008;46. doi:10.1029/2007RG000227.
[47] Karato S, Wu P. Rheology of the upper mantle: A synthesis. Science 1993;260:771–8.
[48] McKenzie DP. Surface deformation, gravity anomalies and convection. Geophys J R Astr Soc 1977;48:211–38.
[49] Solomatov VS. Scaling of temperature- and stress-dependent viscosity convection. Phys Fluids 1995;7:266–74.
[50] Moresi L, Dufour F, Mühlhausi HB. Mantle convection modeling with viscoelastic/brittle lithosphere: Numerical methodology and plate tectonic modeling. Pure Appl Geophys 2002;159:2335–56.
[51] Schubert G, Turcotte DL, Olson P. Mantle convection in the Earth and Planets. Cambridge University Press; 2001.
[52] Turcotte DL, Schubert G. Geodynamics, Application of Continuum Physics to Geological Problems. John Wiley & Sons, New York; 2nd ed.; 2001.
[53] Grinevich PP, Olshanskii MA. An iterative method for the Stokes-type problem with variable viscosity. SIAM J. Sci. Comput. 2009;31:3959–78.
[54] Ritzwoller MH, Shapiro NM, Barmin MP, Levshin AL. Global surface wave diffraction tomography. J Geophys Res 2002;107. doi:10.1029/2002JB001777.
[55] Conrad CP, Lithgow-Bertelloni C. Influence of continental roots and asthenosphere on plate–mantle coupling. Geophys Res Lett 2006;33. doi:10.1029/2005GL025621.
[56] Bird P, Liu Z, Rucker WK. Stresses that drive the plates from below: Definitions, computational path, model optimization, and error analysis. J Geophys Res 2008;113. doi:10.1029/2007JB005460.
[57] Grad M, Tiira T, ESC Working Group . The Moho depth map of the European plate. Geophys J Int 2009;176:279–92.
[58] Bostrom RC. Westward displacement of the lithosphere. Nature 1971;234:536–8.
[59] Doglioni C. The global tectonic pattern. J Geodyn 1990;12:21–38.
[60] Doglioni C. Geological evidence for a global tectonic polarity. J Geol Soc, London 1993;150:991–1002.
[61] Nielsen SB, Stephenson R, Thomsen E. Dynamics of mid-Palaeocene North Atlantic rifting linked with European intra-plate deformations. Nature 2007;450:1071–4.
[62] Wessel P, Smith WHF. New version of Generic Mapping Tools (GMT) version 3.0 released. Eos Trans AGU 1995;76:329–.

MOX Technical Reports, last issues

Dipartimento di Matematica "F. Brioschi",
Politecnico di Milano, Via Bonardi 9 - 20133 Milano (Italy)

12/2011 Miglio E.; Cuffaro M.
Tectonic evolution at mid-ocean ridges: geodynamics and numerical modeling

11/2011 Formaggia, L.; Minisini, S.; Zunino, P.
Stent a rilascio di farmaco: una storia di successo per la matematica applicata

Formaggia, L.; Minisini, S.; Zunino, P.
Stent a rilascio di farmaco: una storia di successo per la matematica applicata

10/2011 Zunino, P.; Vesentini, S.; Porpora, A.; Soares, J.S.; Gautieri, A.; Redaelli, A.
Multiscale computational analysis of degradable polymers

09/2011 Pigoli, D.; Sangalli, L.
Wavelets in Functional Data Analysis: estimation of multidimensional curves and their derivatives

08/2011 Ieva, F.; Paganoni, A.M.; Secchi, P.
Mining Administrative Health Databases for epidemiological purposes: a case study on Acute Myocardial Infarctions diagnoses

07/2011 Arioli, G.; Gamba, M.
Automatic computation of Chebyshev polynomials for the study of parameter dependence for hyperbolic systems

06/2011 Secchi, P.; Stamm, A.; Vantini, S.
Large p Small n Data: Inference for the Mean

05/2011 Arioli, G.; Gamba, M.
An algorithm for the study of parameter dependence for hyperbolic systems

04/2011 Ieva, F.; Paganoni, A.M.; Pigoli, D.; Vitelli, V.
Multivariate functional clustering for the analysis of ECG curves morphology